42 Aero Camino, Goleta, CA 93117
Tel (805) 685-0066 | Fax (805) 685-0067
info@biopac.com | **www.biopac.com**

7/25/22

Application Note 294: Trans-radial Electrical Bioimpedance Velocimetry (TREV)

Blood Flow Measurements using the NICO100D

This application note discusses Trans-Radial-Ulnar Electrical bioimpedance Velocimetry (TRUEV); measurements and analysis; the configuration discussed interrogates both the radial and ulnar (TREV >> TRUEV) arteries.

The following BIOPAC product are referenced in this application note:

- AMI100D Amplifier Module Interface
- ECG100D Electrocardiogram Smart Amplifier
- EL526 Strip Electrodes
- HLT100C High-level Transducer Interface
- IPS100D Isolated Power Supply
- MECMRI-NICO MRI filtered cable sets
- MP160 Data Acquisition System with Acq*Knowledge*
- NICO100C-MRI Noninvasive Cardiac Output Amplifier for MRI
- NICO100D Noninvasive Cardiac Output Amplifier
- PPG100C Photoplethysmogram Amplifier
- TCIPPG3 Nonin 9-Pin to PPG100C Interface
- TSD124D SpO_2 Finger Clip

Topics

Trans-radial Electrical Bioimpedance Velocimetry (TREV)

The term Trans-radial Electrical bioimpedance Velocimetry (TREV) was invented by Dr. Don Bernstein. See Selected References beginning on page 20 for Dr. Bernstein's contributions to advancing the field of bioimpedance-based cardiovascular measures.

The BIOPAC NICO100D module, when used with a range of electrode types, from spots to strips, is suitable for measuring blood movement in the forearm and, by extension, the vascular networks that feed the forearm. This discussion of measurement methods illustrates a range of possibilities.

There are two major arteries in the forearm, the ulnar and the radial. Depending on electrode type and placement, more emphasis can be made on measurement of one artery or the other because the forearm is a volume conductor.

In this document, TREV is shorthand for Trans-Radial-Ulnar Electrical bioimpedance Velocimetry (TRUEV). This discussion utilizes the NICO100D in a configuration that interrogates both the radial and ulnar (TREV >> TRUEV) arteries via four EL526 strip electrodes to measure bioimpedance.

TREV Measurement

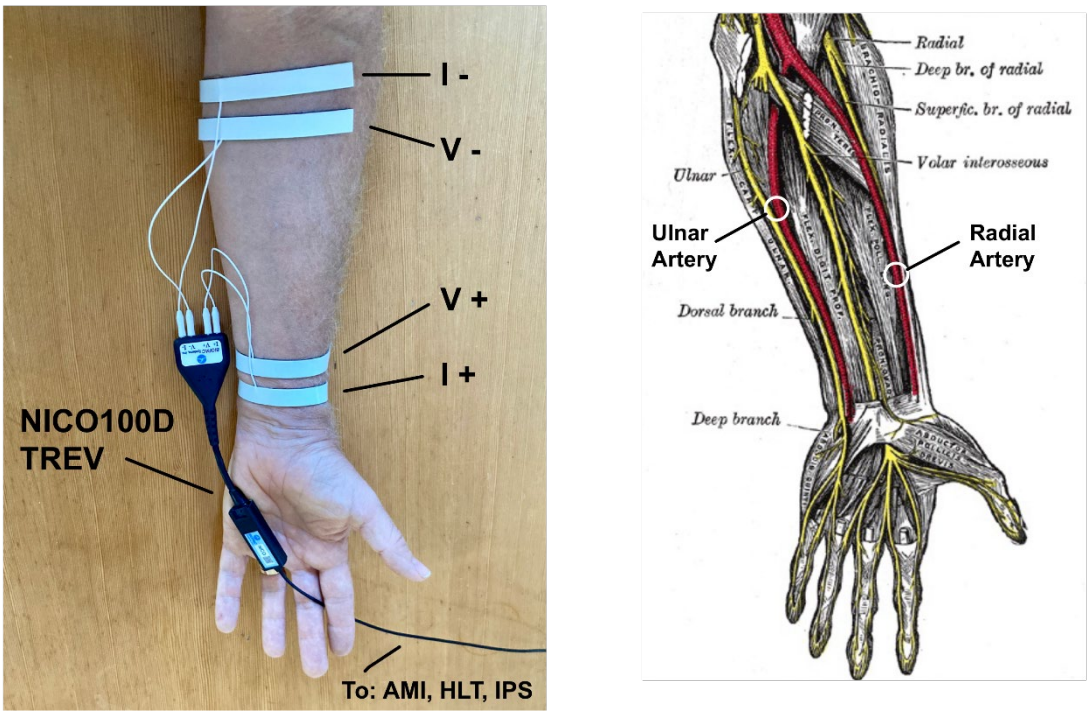

1A 1B

Fig. 1: Placement of the EL526 electrode strips

A NICO100D measurement or TREV produces ohmic equivalents of cardiac-generated blood velocity and acceleration. The integral of blood velocity multiplied by heart rate (HR) results in a signal proportional to cardiac output (CO). The NICO100D obtains a pulsatile cardiac-induced signal from the forearm arteries, thus obviating many errors of the transthoracic method, specifically the complex anatomy associated with the torso. The NICO100D uses a simple strip, four-electrode array on the forearm. It is easy to apply and, unlike transthoracic methods, user-friendly (Fig. 1A, 1B). Note that the radial and ulnar arteries are within the current field (I^- and I^+), as well as the two (2) voltage-sensing electrodes (V^- and V^+). Also note that the forearm radial and ulnar arteries align orthogonally to both the current injection and voltage-sensing electrodes. Since the magnitude of the impedance signal is anisotropic, it depends upon parallel orientation with respect to the applied current to obtain a high signal-to-noise ratio measurement.

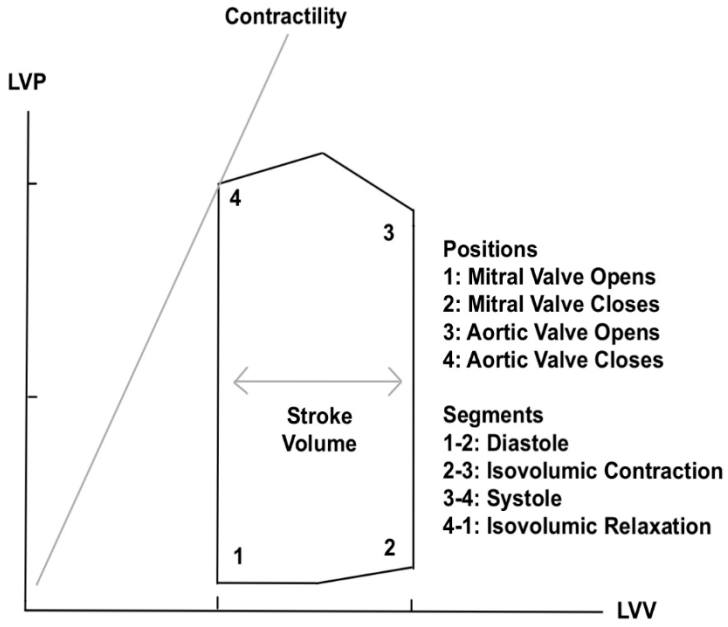

Fig. 2: Frank-Starling Mechanism—relationship between left ventricular pressure and left ventricular volume

Derived Indices Relevant to TREV

- Contractility Index (Jerk): the time-derivative of Acceleration $(\Omega \cdot s^{-3})$
- Acceleration: dZ(t)/dt $(\Omega \cdot s^{-2})$
- Velocity: the integral of Acceleration $(\Omega \cdot s^{-1})$
- The Integral of Velocity (Ω)
- Cardiac Output: Proportional to Integral of Velocity x Heart Rate $(\Omega \cdot HR)$

TREV can be used to generate an index of Contractility (Fig. 2) by simply performing a running derivative on the NICO100D dZ(t)/dt (Acceleration) output.

Measurement Methods: Ergonomics, Electrodes, Amplifier, Data Acquisition, Software

TREV provides useful information concerning blood acceleration, blood velocity, stroke volume, and cardiac output.

Equipment Setup: BIOPAC Systems MP160, AMI100D, NICO100D, ECG100D

Analog Inputs

CH1: Z (Impedance – Z(t))
CH2: dZ/dt (Acceleration – Acc)
CH3: Electrocardiogram (ECG)

Calculation Channels

CH1 > CH40: Z(t)
CH2 > CH41: Acc
CH3 > CH42: ECG
CH42 > CH43: ECG

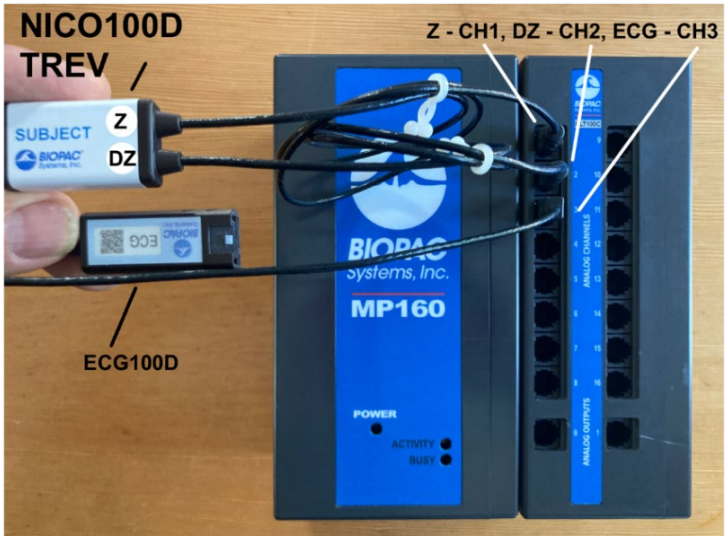

Fig. 3: TREV apparatus

Bioimpedance Equivalents of Hemodynamic Variables for Circulatory System

Blood Velocity: *dZ(t) (ohms/s) – the "Z" output of the NICO100D*

- Blood Acceleration: *dZ(t)/dt (ohms/s^2) – the "DZ" output of the NICO100D*
- Contractility Index: 2nd time-derivative of *dZ(t), (ohms/s^3)*

Bioimpedance Model

Changes in the voltage sensing inter-electrode distance generate concordant changes in the magnitude of the impedance variables.

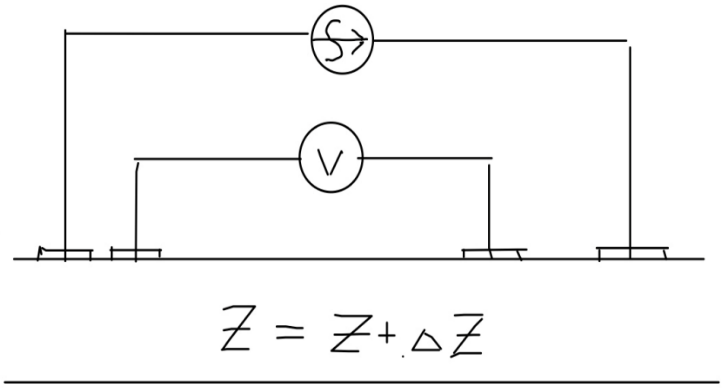

Fig. 4A: Forearm impedance model

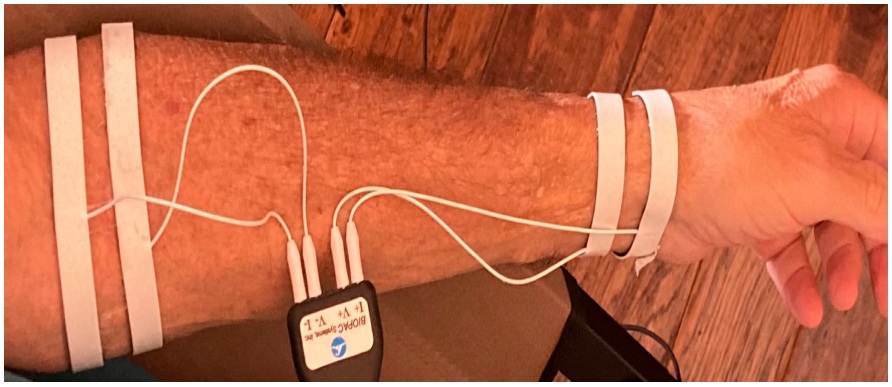

Fig. 4B: TREV Electrode Application

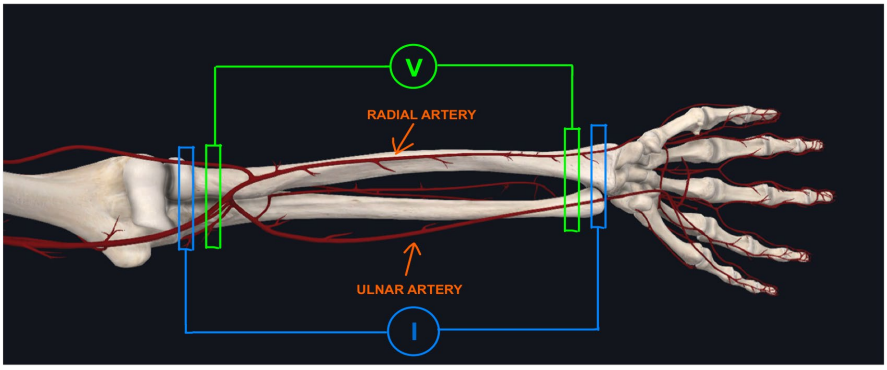

Fig. 4C: TREV schematic and signal representation

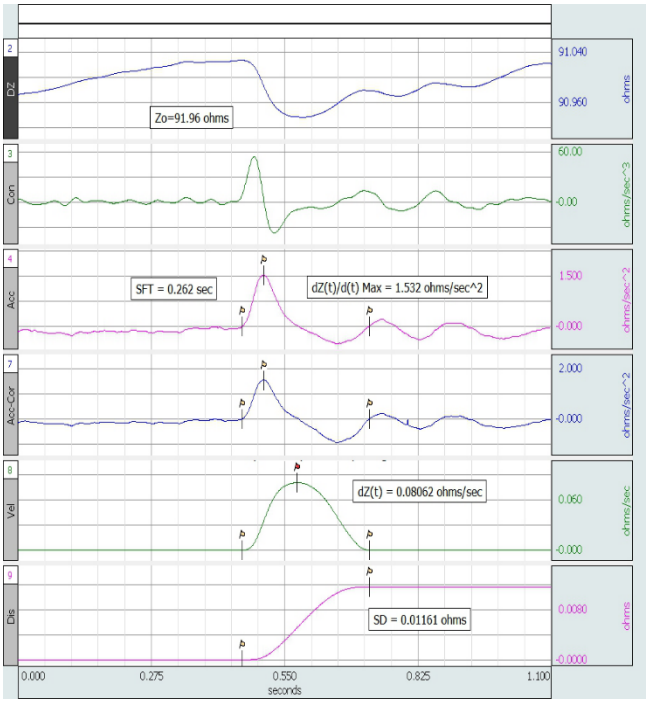

Fig. 5A: 15 cm interelectrode spacing

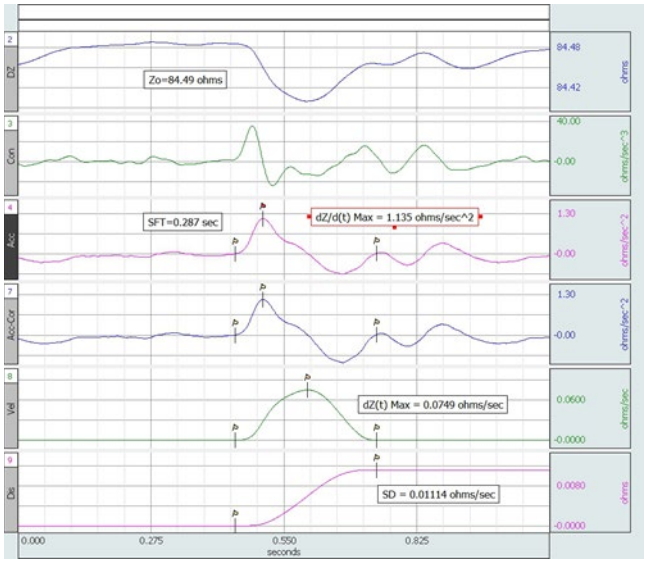

Fig. 5B: 14 cm interelectrode spacing

Hemodynamic Experiments

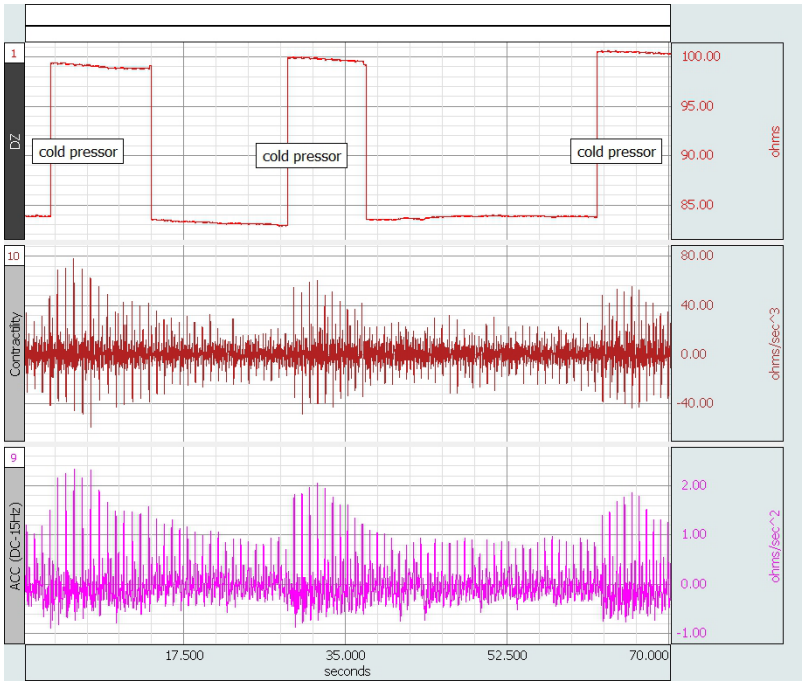

Fig. 6: TREV cold pressor test

In the cold pressor test, a TREV Strip Electrode Array is placed on left arm while the right arm is inserted into an ice bath. Note the considerable increases in Contractility Index—the beat-to-beat maximum peak values in CH 10—after the right arm is inserted into the water/ice bath (Fig. 6).

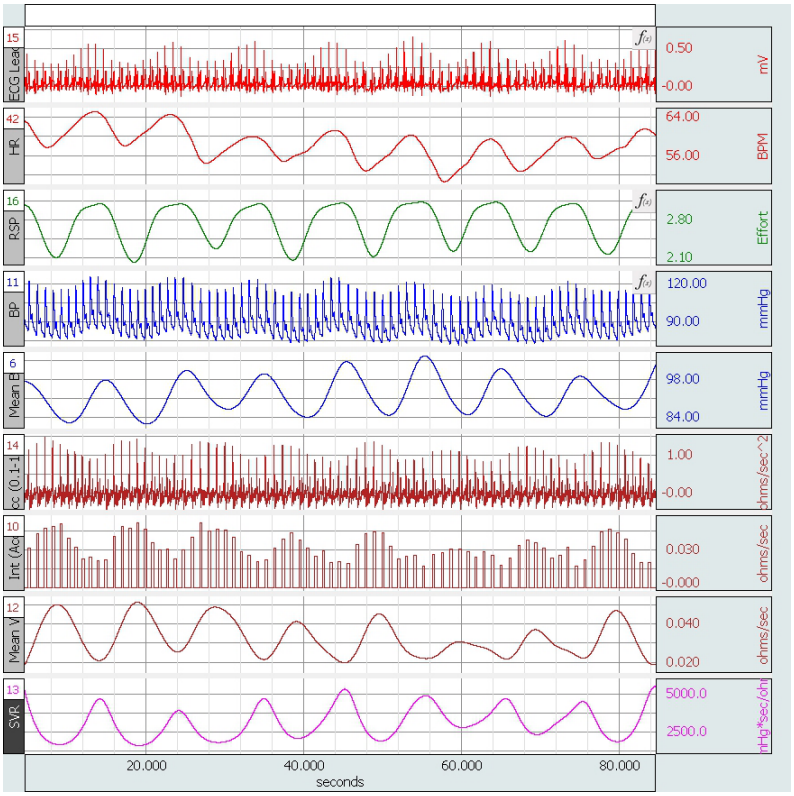

Fig. 7: Respiration, heart rate, blood pressure, blood flow, and SVR

Note the varying phase relationships between heart rate (CH 42), respiration (CH 16), mean blood pressure (CH 6), mean velocity (CH12) and systemic vascular resistance (CH 13) (Fig. 7). Noninvasive Continuous Blood Pressure measurement is performed for validation purposes.

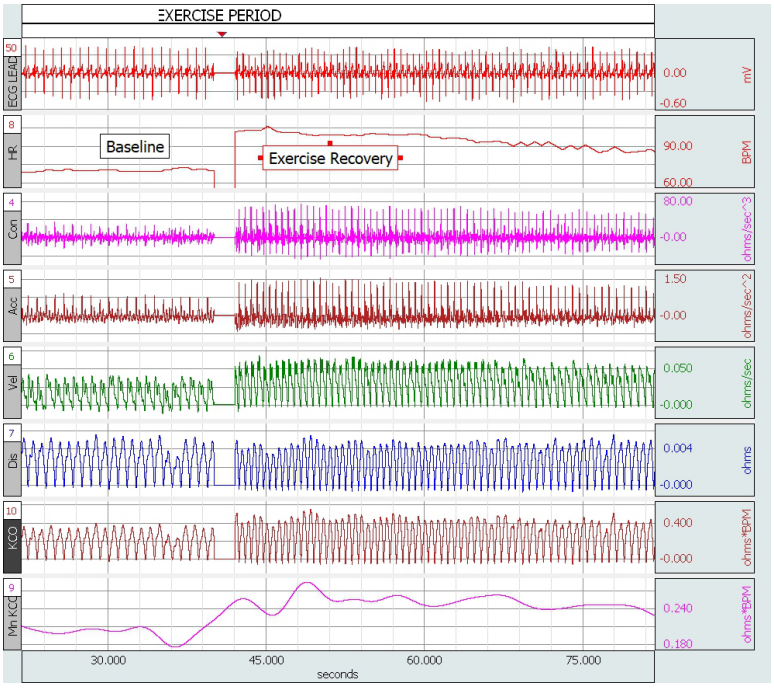

Fig. 8: Exercise – baseline and recovery – cardiac output indicator

The integral of Blood Velocity (CH 7) multiplied by Heart Rate (CH 8) is proportional to Cardiac Output. Note the increase in the Cardiac Output indicator (KCO) after exercise—shown in channels 10 and 9 (running mean of CH 10).

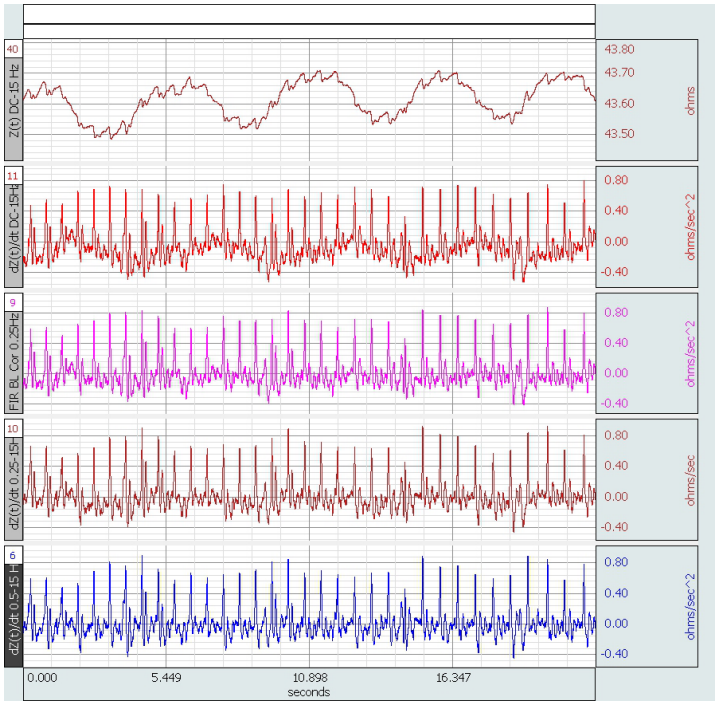

Fig. 9: Baseline correction algorithms for respiratory artifact removal

Respiratory-induced baseline artifact variations should be minimized or eliminated to perform TREV measurements that are specific to cardiac function only. When respiratory baseline artifacts are removed, it is much easier to see variations in cardiac output due to changes in heart pumping performance. Fig. 9 illustrates that the respiratory baseline artifact removal algorithm has no material impact on peak Acceleration magnitudes—the averages of the peak Acceleration values for all the filtered Acceleration waveforms are equivalent (0.75 ohms/sec^2).

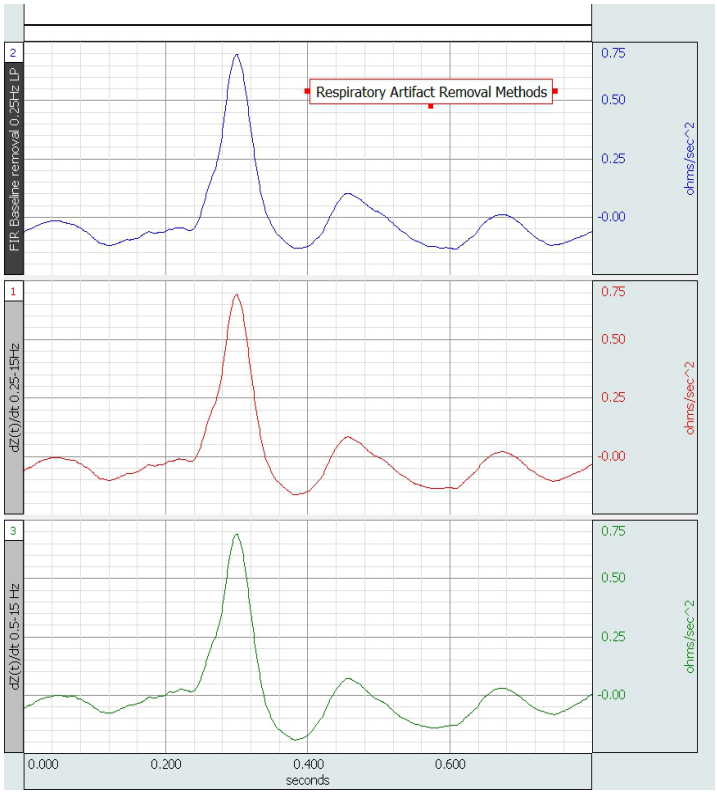

Fig. 10: Comparisons of Accelerations derived from baseline correction algorithms

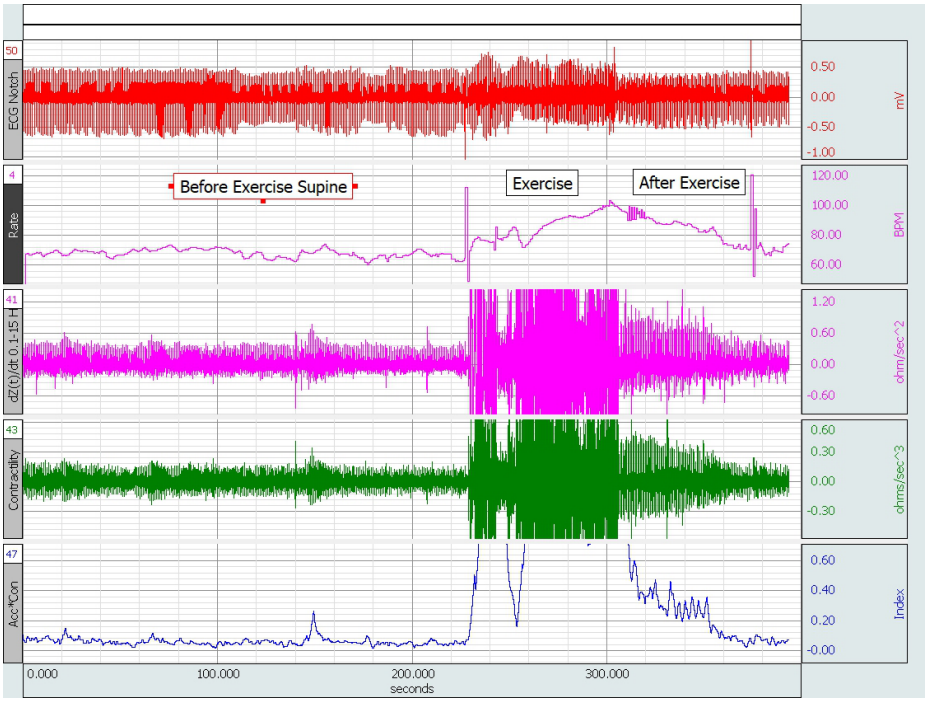

Fig. 11: CAM Index: (Contractility Index - Max) x (Acceleration - Max)—before and after exercise

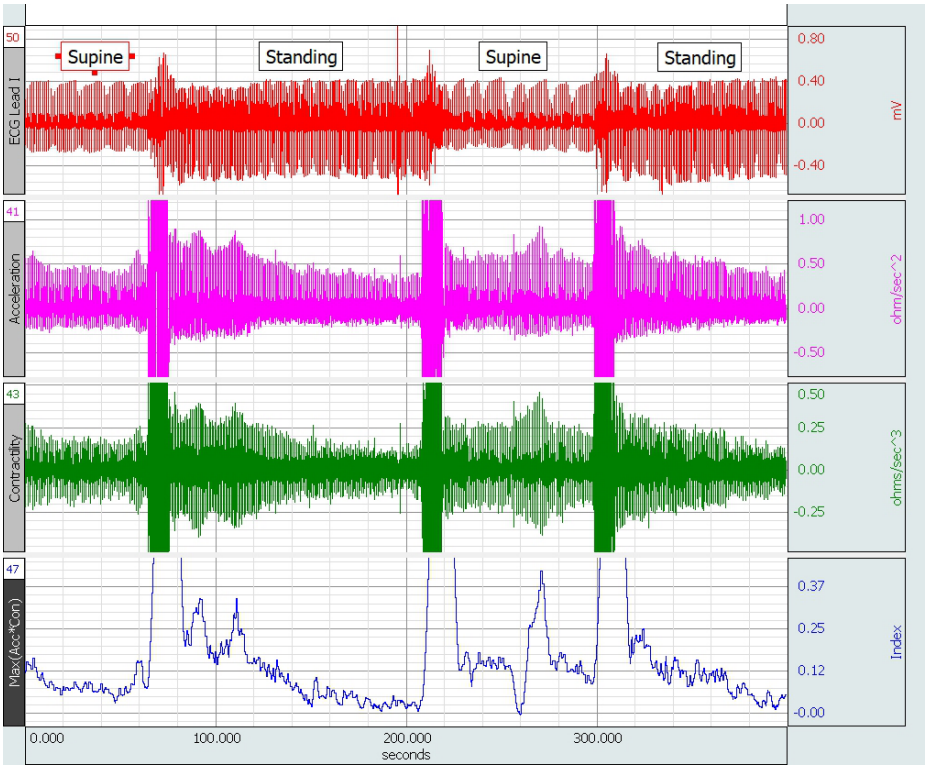

Fig. 12: CAM Index: (Contractility Index - Max) x (Acceleration - Max)—supine and standing

Note: CAM is the “Contractility – Acceleration – Max” Index. CAM is calculated by multiplying the beat-to-beat Acceleration Maximum Peak by the beat-to-beat Contractility Index Maximum Peak. In Fig. 11 and Fig. 12, CAM is shown in CH 47 - bottom channel.

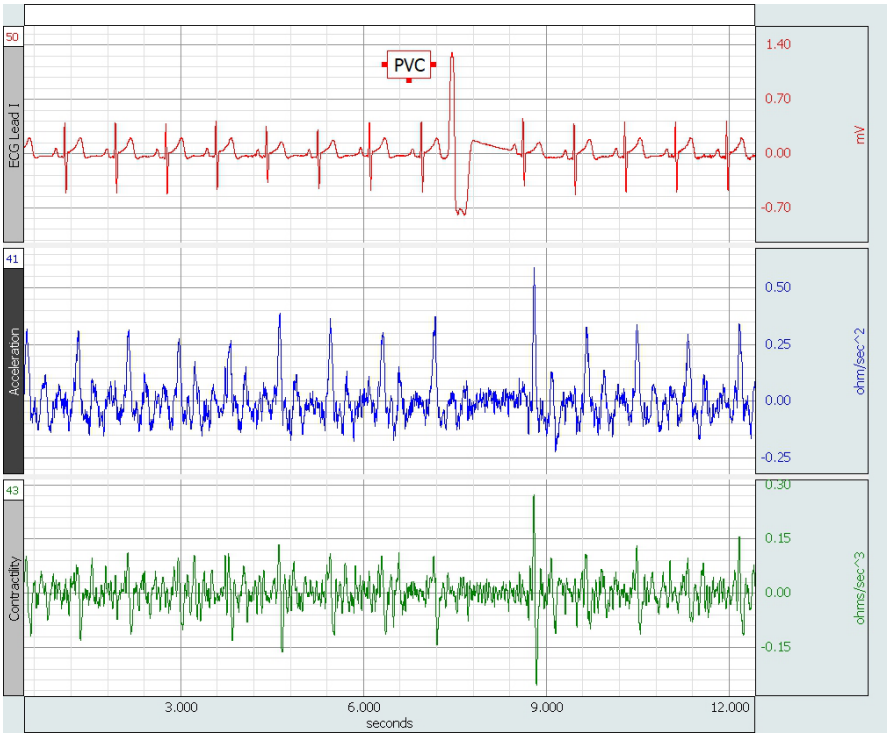

Fig. 13A: Post Extra-Systolic Potentiation

Premature ventricular contraction (PVC) Occurrence Phenomena: Note that after the PVC, there is a latency period (compensatory pause), followed by an enhanced value for Acceleration and its derivative, (Contractility Index).

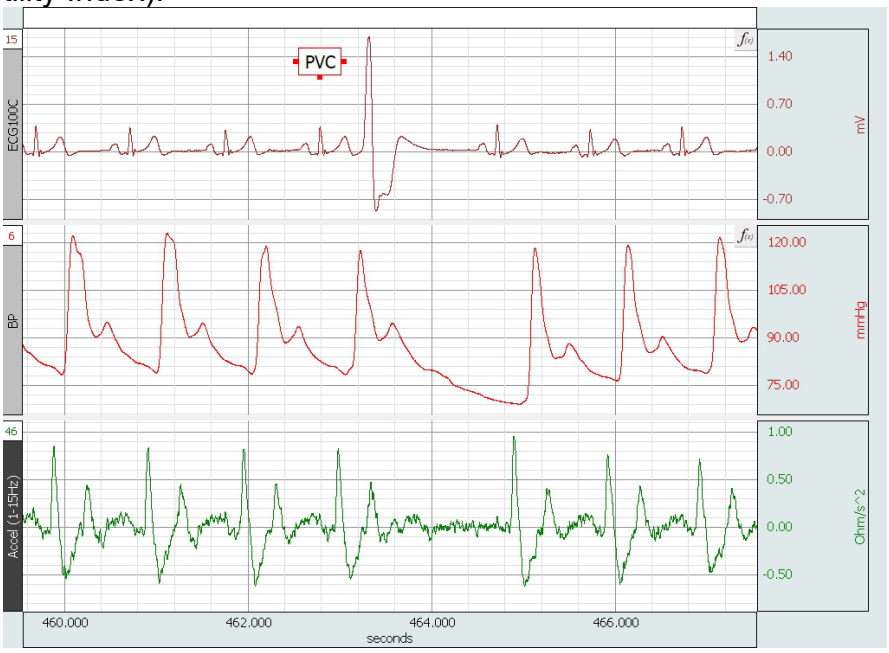

Fig. 13B: Post Extra-Systolic Potentiation

PVC Occurrence Phenomena: Note compensatory pause, followed post extra-systolic potentiation in Fig. 13A. Blood pressure (BP) (CH 6) is collected for validation purposes.

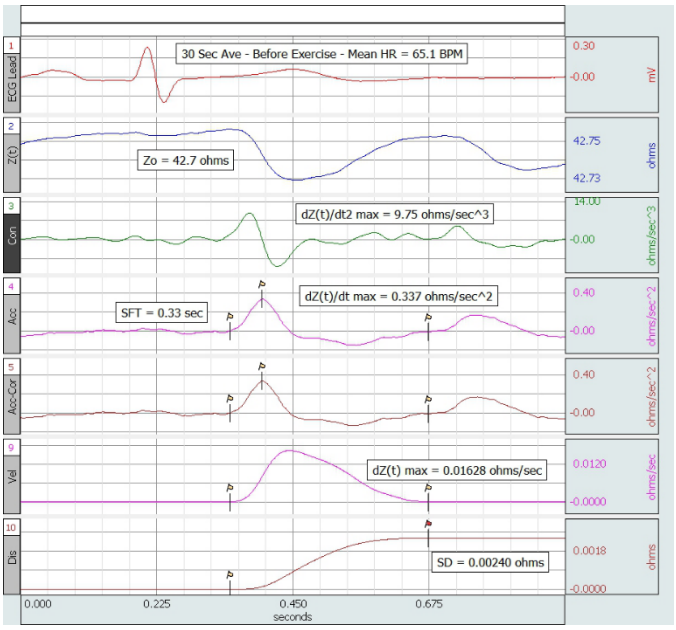

Fig. 14A: Before exercise

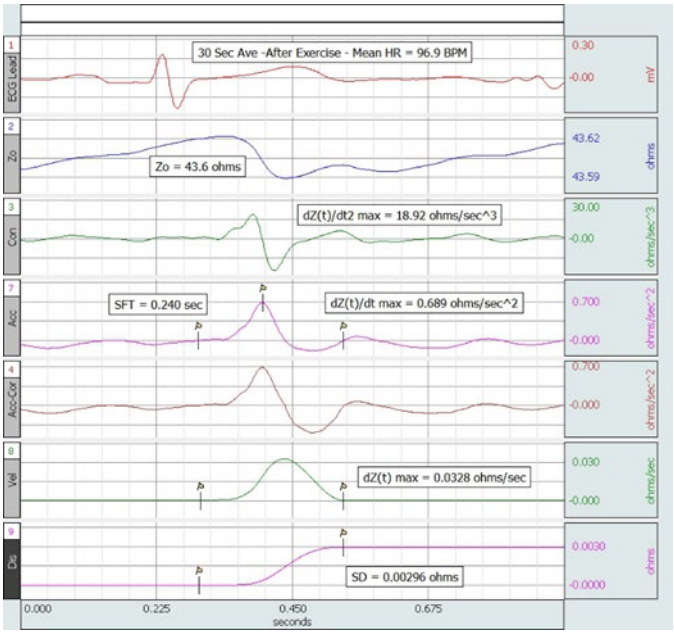

Fig. 14B: After exercise

Contractility Index, Acceleration, and Velocity increase after exercise (Fig. 14B). Also, the integral of blood velocity changes only slightly because the area beneath the curve has decreased significantly, despite a higher peak blood velocity. This is due to a significantly shortened systolic flow time (SFT) after exercise, which is a function of increased heart rate. This is consistent with the observation that SV shows insignificant change with mild to moderate exercise. Despite increased (Contractility Index), the integral of blood flow (proportional to stroke volume) does not change, principally due to decreased SFT.

Grip Anticipation Test

In this test, the subject is required to periodically deliver a high-exertion grip. The subject is asked to squeeze the hand dynamometer as quickly and with as much pressure as possible every two minutes.

Trial A is the first grip test. Trial B is the second grip test.

The hand dynamometer is measured in CH 4. Blood acceleration (dZ(t)/dt) is measured in CH 41. CH 6 represents the running cyclic Acceleration Standard Deviation value. This could also be configured as the running cyclic Acceleration Peak value, as results appear to correlate proportionally.

The Contractility Index is the derivative of Acceleration. CH 7 shows the running cyclic Contractility Index Standard Deviation. Similarly, this could also be configured as the running cyclic Contractility Index peak value, and again results appear to correlate proportionally. At about 30 seconds prior to the grip, both tests (A and B) mark the beginning of a rapid increase in both Acceleration and Contractility Index.

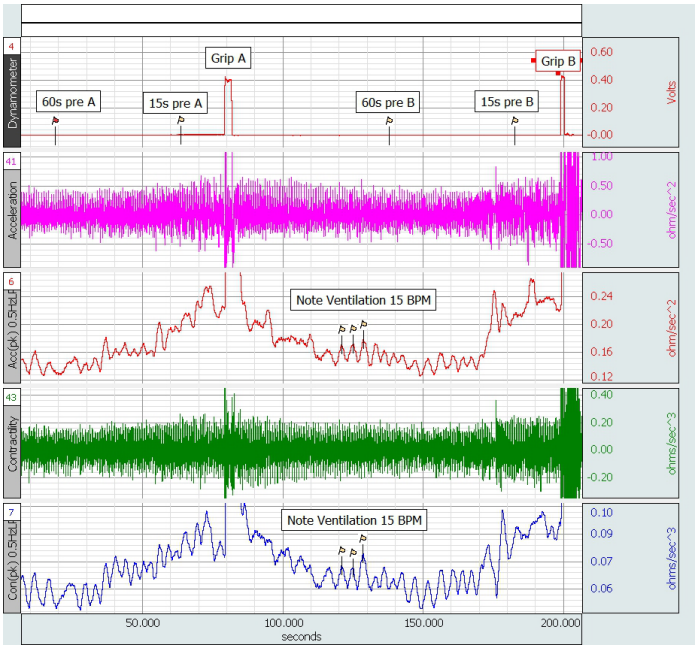

Fig. 15: Cycle by Cycle Peak Acceleration and Contractility Index

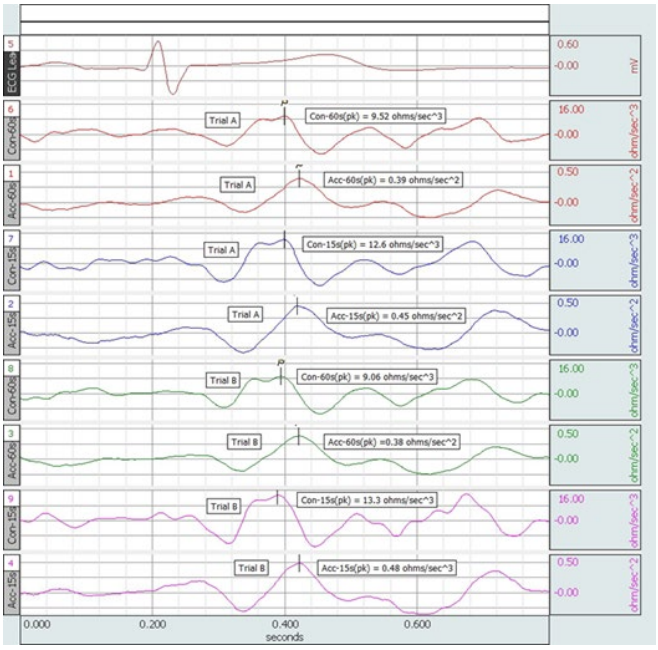

Fig. 16: Acceleration and Contractility Index—10-beat average

Increases in Acceleration and Contractility Index can be noted at 15 seconds prior to grip exertion, compared to baseline values at 60 seconds prior to grip exertion. Contractility Index in the 15 seconds just prior to grip task averages 139% higher than Contractility Index from 60 seconds to 45 seconds prior to the grip task. Also, note that ventilatory activity registers very clearly on Contractility Index measures. Contractility Index was 9.06 to 9.52 ohms/sec^3 at 60 seconds prior to grip, and it was 12.6 to 13.3 ohms/sec^3 in the 15 seconds immediately prior to grip.

There are significant increases in Acceleration and Contractility Index at 15 seconds (15s pre-A/B) prior to grip exertion, compared to the baseline values at 60 seconds (60s pre-A/B) prior to grip exertion. The mean standard deviation in Contractility Index in the 15 seconds just prior to grip task averages 139% higher than the mean standard deviation in the Contractility Index, from 60 seconds to 45 seconds prior to the grip task, considering the two tests.

Peak Contractility Index was in the range of 9.06 to 9.52 ohms/sec^3 at 60 seconds prior to grip, and it was in the range of 12.6 to 13.3 ohms/sec^3 in the 15 seconds immediately prior to grip. Also, note that ventilatory activity registers clearly in the TREV-derived Contractility Index measures.

TREV - ECG - PPG Timing Measures

In evaluating the timing between TREV [Z(t), Acceleration and Contractility Index], ECG, and Photoplethysmogram (PPG). TREV is measured on the left forearm; ECG is LEAD I and PPG on left index finger. For the 12-second recording, PPG BP (CH 5) is the bandpass (5–15 Hz) of the raw PPG data in CH 4. SFT is approximately the period (~300 ms delta) between the two consecutive PPG BP peaks after R-wave occurrence. Also, note that peak Contractility Index occurs at 170 ms after R-wave peak, and prior to any detection of blood movement, via PPG sensor in CH 2 and CH 3 of the 10-beat averaged data. Pulse PPG was recorded using BIOPAC TSD124D Finger Clip (transmissive sensor) and PPG100C with TCIPPG3 adapter.

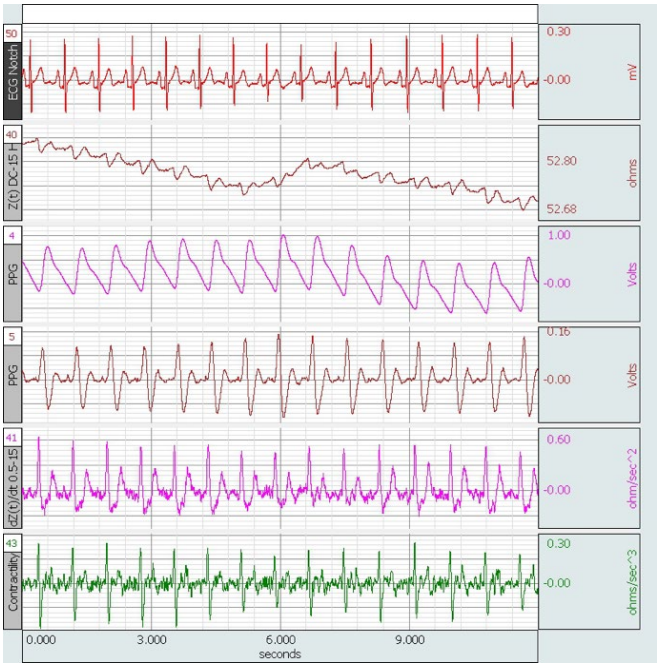

Fig. 17: ECG-Z(t)-PPG- PPG BP-ACC-CON Raw data collection (12-second recording)

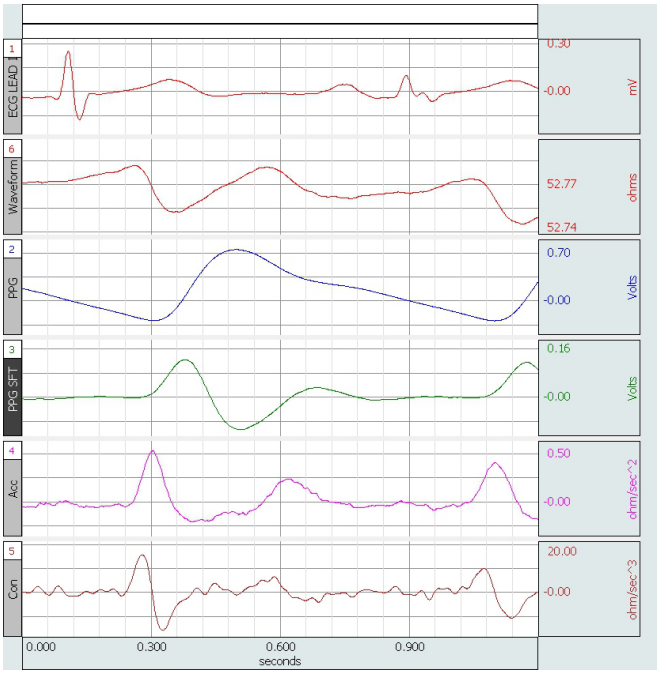

Fig. 18: ECG-Z(t)-PPG- PPG BP-ACC-CON—10-beat average

TREV, ECG, PPG, PWV, BP

Based on TREV's ability to detect blood flow in the forearm, a downstream Blood Volume Pulse sensor could be used to detect the arrival time of the previously measured blood flow. To better identify the arrival time of the blood flow in the thumb, a derivative was applied to the PPG signal. Arrival time minus TREV recording time equals the Pulse Transit Time (PTT). The PWV (inversely proportional to BP) is Distance Traveled / PTT.

In this circumstance, TREV was performed on left forearm, ECG is LEAD I, and a PPG sensor was placed on the left thumb. The thumb artery is not obstructed by the upstream vasculature, and it is not as subject to vasoconstriction as the fingers. Pulse Wave Velocity was measured over the distance from the TREV measurement center point to the thumb.

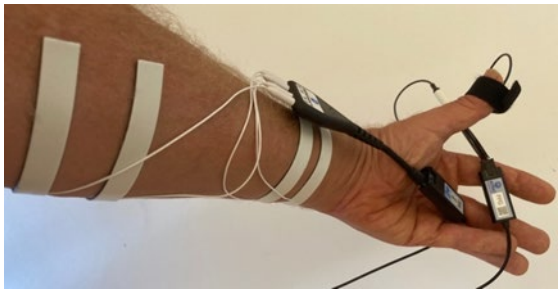

Delta Distance: 25 cm (0.25 meters)
Delta time: 75 ms (0.075 sec)
PWV = 0.25/0.075 = 3.33 meters/sec (nominal)

The delta time was indexed between the Acceleration peak and the first peak of the processed PPGSFT (5–15 Hz BPF applied to PPG). PPGSFT is an optimized derivative of the PPG measurement. The cycle-by-cycle time delta (PTT) was determined and then the results were smoothed using a 0.3 Hz FIR LPF. The PTT measurement was inverted and then scaled to a typical mean blood pressure range (CH 6). The P-MBP (Mean Blood Pressure derived from PTT) peaks were flagged. In Fig. 19A, note the phase relationships between the waves (HR, R pk, Z(t), P- MBP). Fig. 19B shows a 75 ms latency between the Acceleration Peak and the PPGSFT Peak. The Pulse Plethysmogram (PPG) was recorded using BIOPAC's TSD124D Finger Clip (transmissive sensor) and PPG100C with TCIPPG3 adapter.

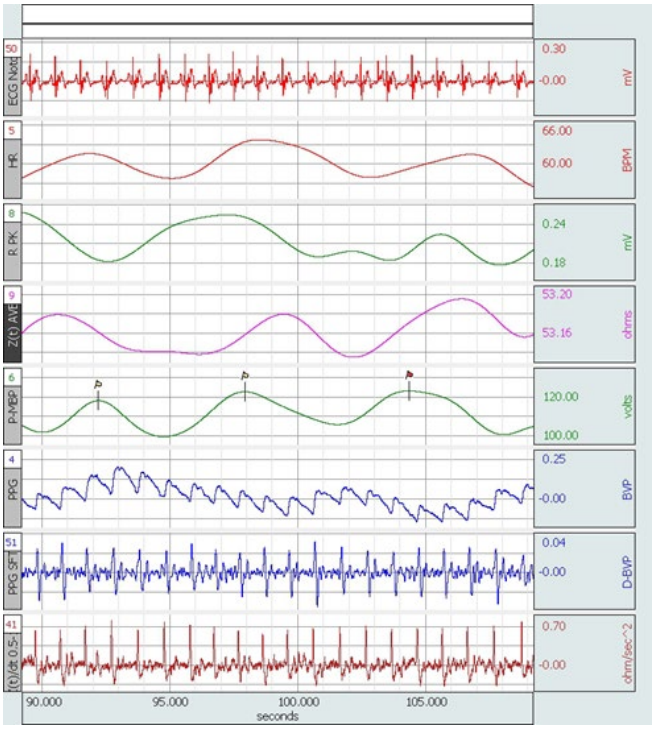

Fig. 19A: ECG-HR-RPK-ZT-PMBP-PPG-PPGSFT-ACC

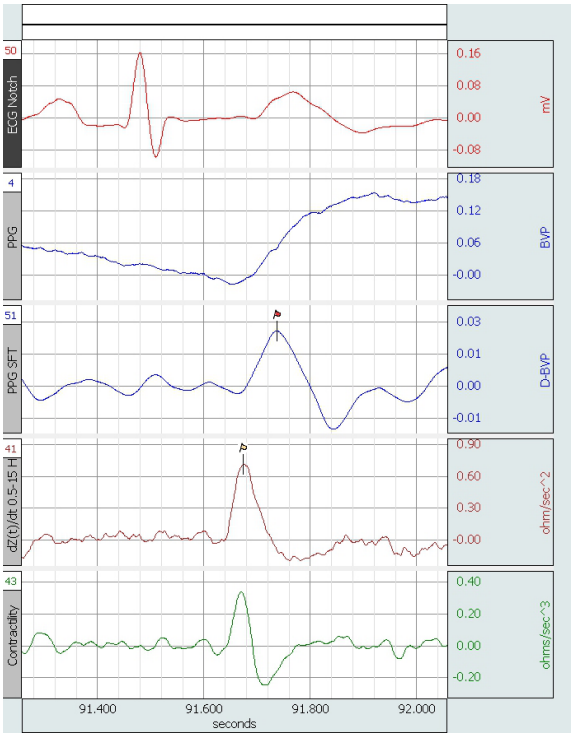

Fig. 19B: Time Delta between Acceleration and PPGSFT

Recording during Breath Holding: ECG, HR, PPG, Z(t), ACC, CON, ACI

In this recording, the participant held their breath on three separate occasions. In Fig. 20, note increases in both Acceleration and Contractility Index at the point breathing resumes. The Acceleration - Contractility Index (ACI) is shown in the bottom waveform (CH 47). Ventilatory effort is reflected in the baseline variations of Z(t). In addition to the increases in the ACI after ventilation resumption, ACI also increases after the longer-term drops in Blood Volume Pulse (PPG - CH 4) baseline.

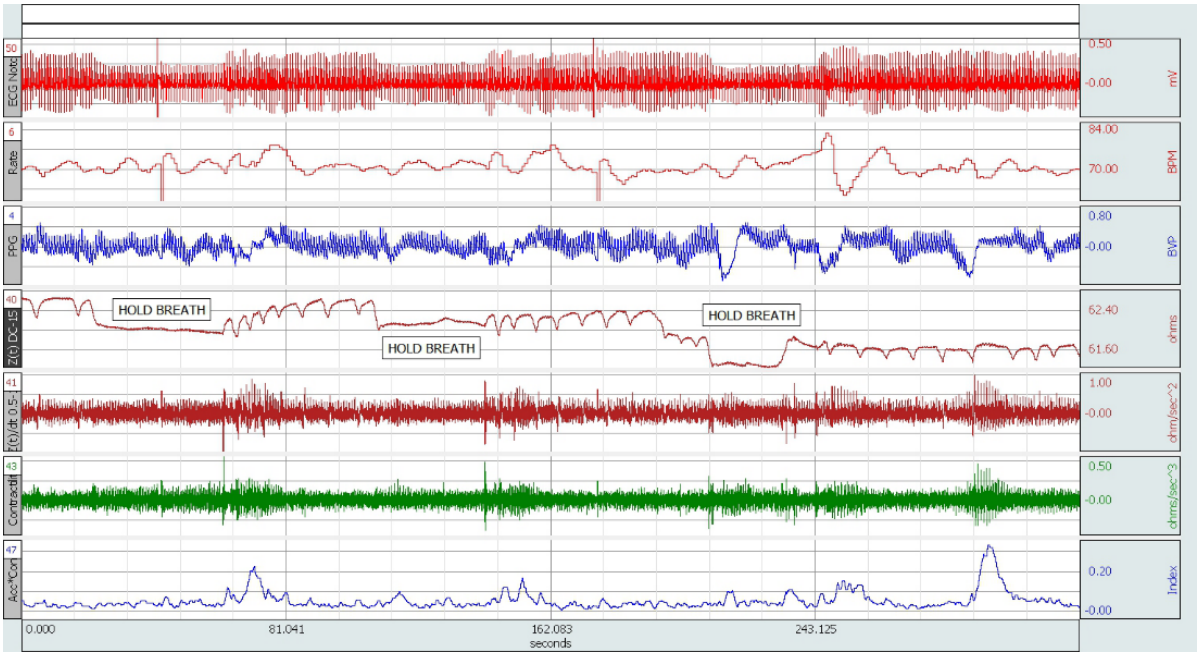

Fig. 20

TREV in the fMRI

TREV was employed on the left forearm of a participant scanned in a Siemens Prisma fMRI. The TREV electrode array consists of four EL526 specialized strip electrodes. Each disposable strip electrode is 1.3 cm wide x 16.7 cm long and incorporates an attached carbon composition lead wire. The four strip electrodes are connected to an MRI-conditional cable assembly through a patch panel MRI filter and then to an MRI control room cable (collectively BIOPAC Systems MECMRI-NICO MRI filtered cable sets) attached to a NICO100C-MRI Noninvasive Cardiac Output Amplifier for MRI. No other equipment was attached to the participant. Various scanning modalities were tested, including axial and coronal Echo Planar, 3-D MPRAGE, T2, and Diffusion Imaging, primarily with multi-band protocols.

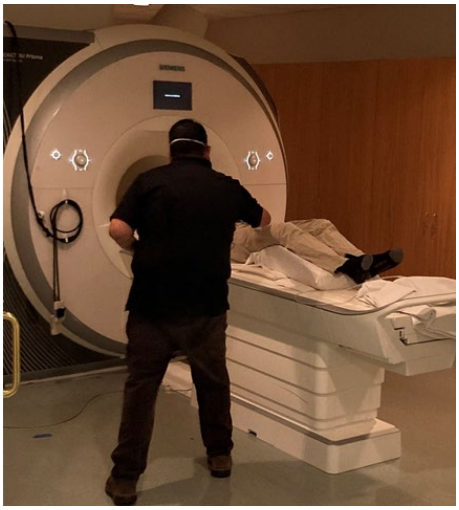

Fig. 21: Siemens Prisma fMRI

The TREV strip electrode array was attached to the left forearm (Fig. 4a). TREV is collected by the application of a 100 kHz sinusoidal current that's introduced through the forearm (schematic electrodes in blue), while the generated 100 kHz voltage is simultaneously measured (schematic electrodes in green). The magnitude of the measured voltage divided by the magnitude of the known current is the magnitude of the bioimpedance [Z(t)] of the measured forearm volume. The measured forearm volume is the volume between the inner voltage-sensing electrodes (Fig. 4a, 4b, and 4c).

The following graph shows the collected TREV data (Fig. 22). Impedance [Z(t)] is the top channel (red) and has units of ohms/sec. The bottom channel (blue) is the derivative of Z(t) or dZ(t)/dt, referenced as Acceleration (ACC), and has units of ohms/sec^2. Contractility Index (not shown), the derivative of Acceleration, is defined as d2Z(t)/dt2 and has units of ohms/sec^3.

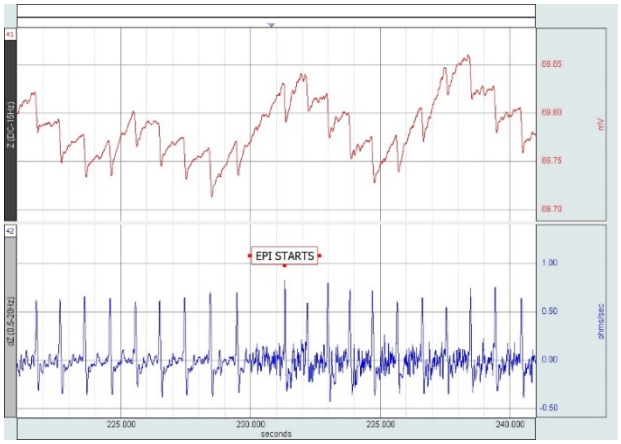

Fig. 22: Measured TREV – EPI axial scan, multi-band

Coincidental with the onset of EPI, baseline noise is observed in the Acceleration waveform (blue). However, the peak Acceleration values are still easily marked. Accordingly, by employing beat-by-beat signal averaging time-aligned to the Acceleration peak values, the Acceleration waveform resolution can be greatly improved, even when averaged over just a few beats.

As an aside, note that a PVC occurred just after the onset of EPI. The missing beat is easily seen and the Acceleration peak, following the PVC, is boosted in comparison to the Acceleration peak just prior to the PVC.

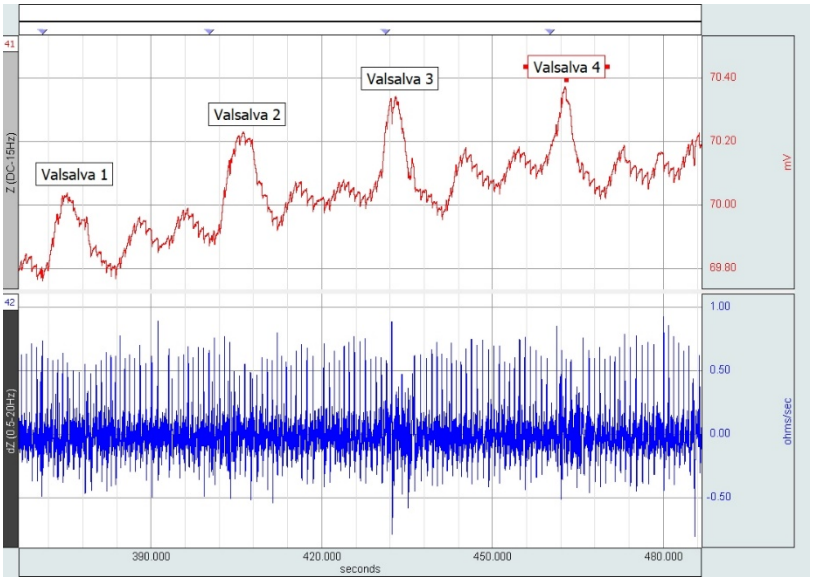

Fig. 23: Four consecutive Valsalva Maneuvers and Recovery Periods

Each Valsalva Maneuver is reflected as a temporary increase in the baseline impedance [Z(t)] and a corresponding decrease in the Acceleration peak values during the Maneuver period. Directly after the Maneuver is finished, the Recovery period shows a relative increase in the measured Acceleration peak values. The Impedance [Z(t)] waveform has units of ohms/sec. The Acceleration (dZ(t)/dt) waveform has units of ohms/sec^2.

For the purposes of this study, five consecutive beats were averaged during the Valsalva Maneuver Period and five consecutive beats were averaged during the Recovery Period.

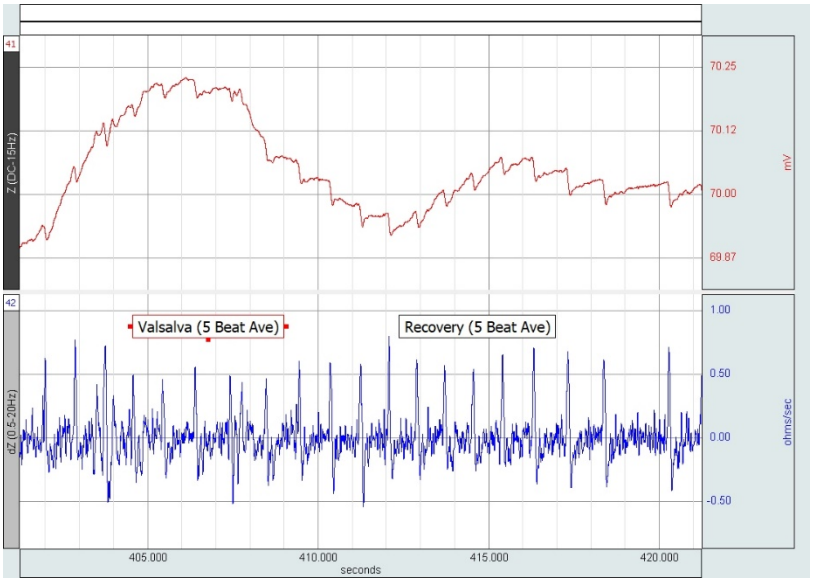

Fig. 24: Detailed view of Valsalva Maneuver and Recovery Period to obtain five-beat averages

During the Valsalva Maneuver, the Acceleration peak values are collectively suppressed. During the Recovery Period, the Acceleration peak values are collectively higher. Impedance [Z(t)] waveform units are in ohms/sec. Acceleration waveform units are in ohms/sec^2.

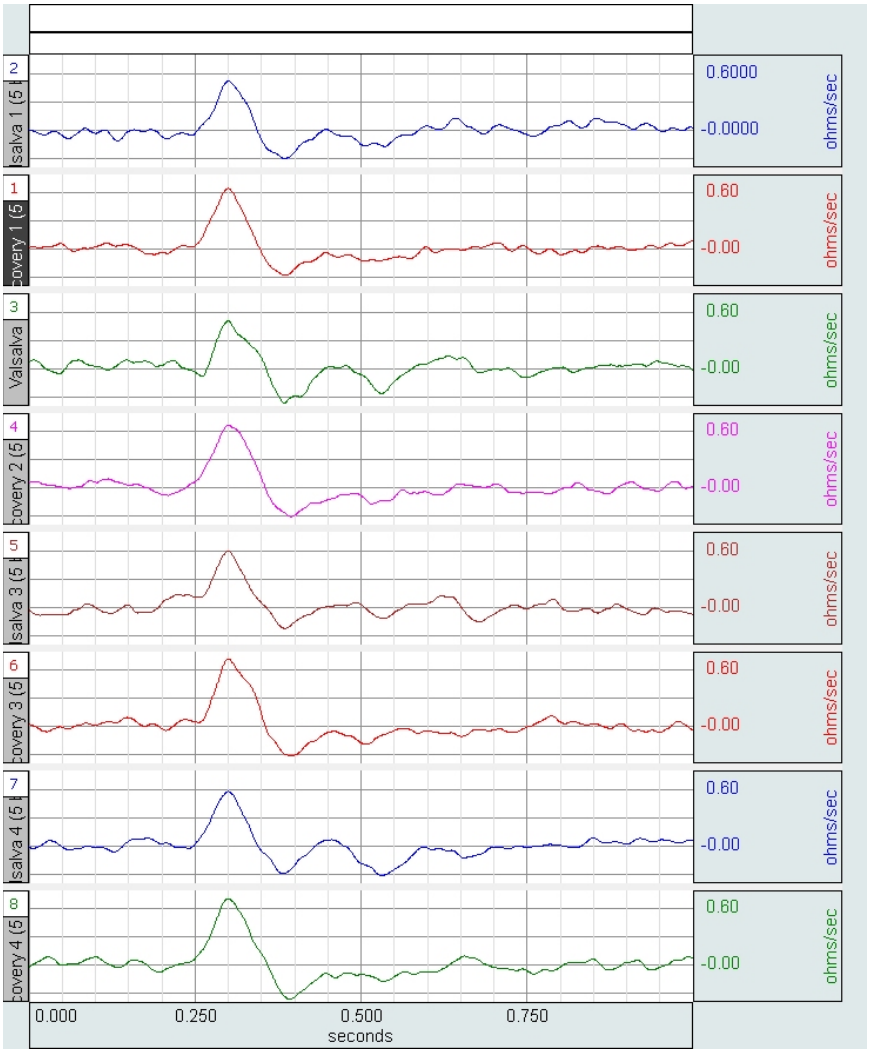

Fig. 25: Individual trial averages for consecutive Valsalva Maneuvers and Recovery Periods

Due to the five-beat signal averaging employed, waveform resolution is substantially improved. Units of all the Acceleration waveforms are ohms/sec^2. The Valsalva Maneuver acts to reduce stroke volume during the maneuver and then stroke volume increases afterwards.

The first (top), third, fifth, and seventh Acceleration waveforms are representative of the Valsalva Period Trial Averages. Note that all Acceleration peaks are at or less than 0.60 ohms/sec^2.

The second, fourth, sixth, and eight (bottom) Acceleration waveforms are representative of the Recovery Period Trial Averages. Note that all Acceleration peaks are greater than 0.6 ohms/sec^2.

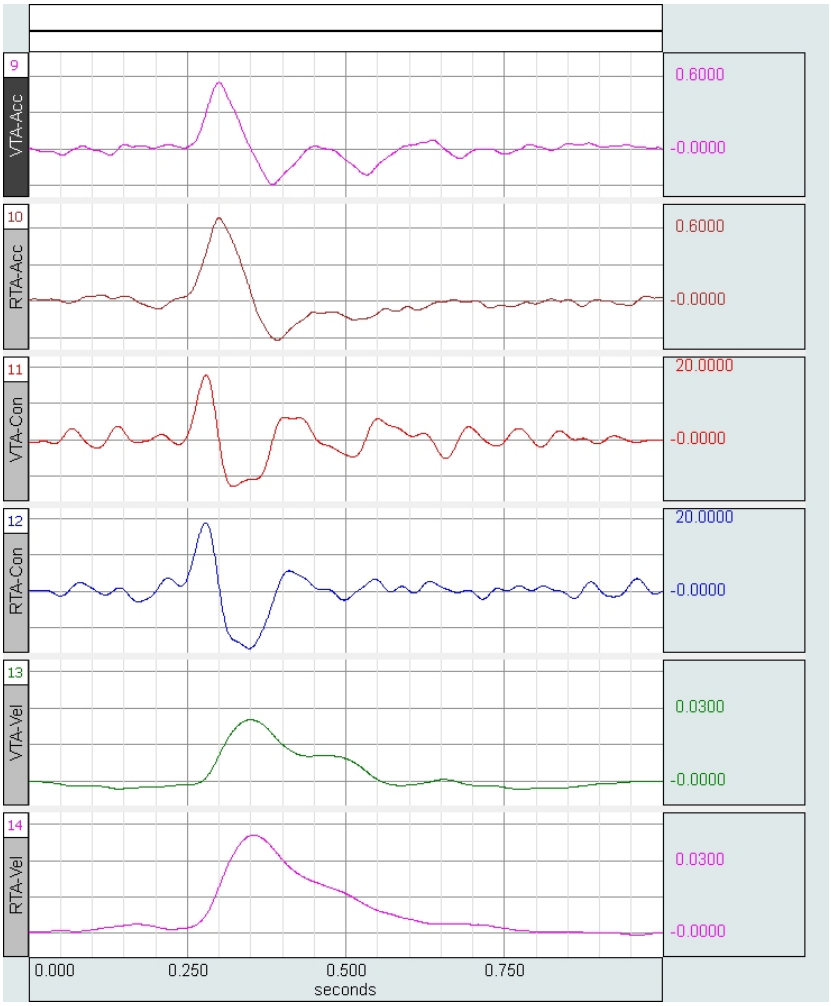

Fig. 26: Collective averages—Valsalva / Recovery Periods for Acceleration, Contractility Index and Velocity

The first (top) waveform is the Acceleration waveform for the Valsalva Trial Average (VTA) for four Valsalva Period Trials. Accordingly, this represents a collective 20-beat average, given that a single Valsalva Period Trial averages five beats.

The second waveform is the Acceleration waveform for the Recovery Period Trial Average (RTA) for four Recovery Period Trials. Accordingly, this represents a collective 20-beat average, given that a single Recovery Period Trial averages five beats. Acceleration waveforms are in units of ohms/sec^2.

The third waveform is the Contractility Index waveform for the VTA. The fourth waveform is the Contractility waveform for the RTA. Contractility Index waveforms are in units of ohms/sec^3.

The fifth waveform is the Velocity waveform for the VTA. The sixth (bottom) waveform is the Velocity waveform for the RTA.

Velocity waveforms are in units of ohms/sec.

IMPORTANT: The positive peak of the Contractility Index is coincident with the onset of the blood Velocity waveform. Contractility Index peaks PRIOR to any movement of blood in the measured volume.

There is very little difference between the Contractility Index maximum peak values between the Valsalva and Recovery Period Trial Averages. This indicates that the Contractility Index is largely unaffected by pre-load and is the ohmic image of isovolumic dP(t)/dt max.

There is a modest increase (~15%) in the Acceleration peak values from the VTA to RTA.

There is a substantial increase (~60%) in the Velocity peak values from the VTA to RTA.

The Integrated Velocity waveform, from the first upward zero-crossing to first downward zero-crossing of the Velocity waveform, reflects Stroke Volume. The Stroke Volume of the RTA shows a 90% increase over the VTA.

Despite the consistency of the Contractility Index from the Valsalva Period to the Recovery Period, there is a significant increase in Blood Velocity and a more significant increase in the integral of Blood Flow (proportional to Stroke Volume) during the Recovery Period as compared to the Valsalva Maneuver Period.

Tilt Table Test

In this test, the participant was placed on a tilt table. The initial measurements were made with the participant in a horizontal position. For subsequent measurements, the participant was tilted at a 45° angle with feet closer to the floor. Measurements consisted of Base Impedance (CH 40), Acceleration (CH 41), and the Pulse Plethysmogram (CH 42). Acceleration, Cycle by Cycle, Maximum (CH 3) and Pulse Rate (BPM) were derived from the source data in real time. The TREV-related measures were performed on the left forearm, kept level with the heart in both the horizontal and tilted positions.

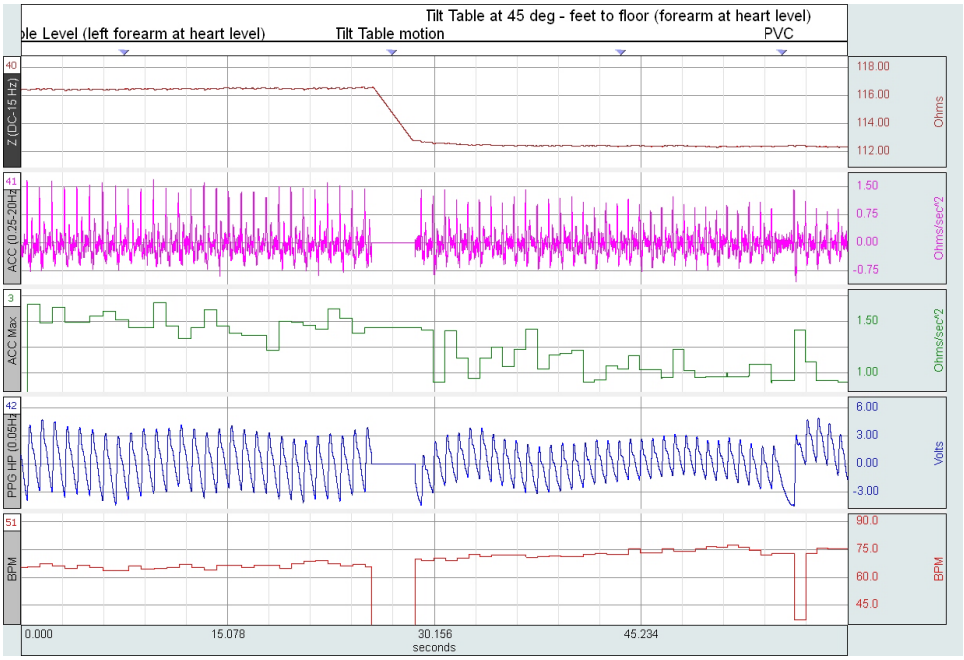

Fig. 27: Tilt Table horizontal and then 45°

The horizontal measurements are in the 0–26 second range. The 45° tilt measurements are in the 28–60 second range. Note the following:

1) Base Impedance [Z(t)] is slightly lower in the tilted position
2) Acceleration maxima are reduced in the tilted position
3) Pulse Plethysmogram peak-to-peak amplitude is reduced in the tilted position
4) Pulse Rate is slightly elevated in the tilted position

Discussion

This measurement demonstrates that when preload decreases as a function of blood pooling in the lower extremities due to the 45° tilt, peak Acceleration (CH 41 and CH 3) decreases because it is preload-dependent. Also, note that the pressure-dependent PPG peak-to-peak (CH 42) decreases as a function of gravitational displacement. As arterial pressure is a function of force F applied to the internal surface area A of vessel walls, the decrease of F is due to decreased mass (i.e., blood),

gravitational acceleration remaining unchanged in the heart and upper extremity. Because F=ma, the mass of blood decreases, so the blood pressure and the pressure-dependent PPG will decrease.

The pulse rate increase from the horizontal to tilted positions is entirely physiologic. As carotid artery pressure decreases, the baroreceptors sense a decrease and cause vagal suppression. This action causes sinus node suppression. Vagal suppression permits the cardio-accelerator adrenergic nerves (T-1 through T-4) to stimulate the heart without the countering effect of sinus node inhibition of heart rate.

As blood pressure diminishes, the carotid baroreceptors, located at the junction of the bifurcation of the common carotid artery into the internal and external branches, send a signal via the Nerve of Hering to the vagal nucleus in the brain. Stimulation of Nerve of Hering inhibits discharge of vagal impulses to the sinoatrial node in the right atrium. Since the SA node induces decreases in heart rate, its inhibition allows the cardio-accelerators, emanating from the thoracic spinal cord, to increase adrenergic stimulation of the heart, effectively increasing heart rate. The increase in heart rate partially compensates for diminished stroke volume to partially maintain cardiac output.

Selected References

Antonini L, Auriti A, Pasceri V, et al. Optimization of the atrioventricular delay in sequential biventricular pacing: physiologic bases, critical review, and new purposes. *Europace* 2012; 14:929-938

Bernstein DP. Method and apparatus for determination of left ventricular stroke volume and cardiac output using the arteries of the forearm. US Patent No. US 9,451, 888 B1, Date of Patent Sep. 27, 2016

Bernstein DP et al. Apparatus and Method for determining an approximation of the stroke volume and cardiac output of the heart. Patent No.: US 6,5111,438 B2. Date of Patent: 28 Jan 2003

Bernstein DP. Apparatus for determination of stroke volume using the brachial artery. Patent No.: US 7,261,697. Date of patent: 28 Aug 2007

Bernstein DP. Apparatus and method for determination of stroke volume using the brachial artery. Patent No.: US 7,806,830 B2. Date of Patent: 5 Oct 2010.

Bernstein DP. Method and Apparatus for determination of left ventricular stroke volume and cardiac output using the arteries of the forearm. Patent No.: US 9,451,888 B1. Date of patent: 27 Sept 2016

Bernstein DP. Method and Apparatus for determination of left ventricular stroke volume and cardiac output using the arteries of the forearm by means of integration technique. Patent No.: US 10,524,668 B2. Date of patent: 7 January 2020.

Bernstein DP, Lemmens HJ. Stroke volume equation for impedance cardiography. *2005 Med. Biol. Eng Comput* 2005; 4:443- 450

Bernstein DP et al. Validation of stroke volume and cardiac output by electrical interrogation of the brachial artery in normals: assessment of strengths, limitations, and sources of error. *J Clin Monit Comput.* 2015; 29:789-800.

Bernstein DP, Impedance cardiography: pulsatile blood flow and the biophysical and electrodynamic basis for the stroke volume equations *2010 J Electr Bioimp* 2010; 1:2-17

Bertini M, Delgado V, Bax JJ, et al. Why, how and when do we need to optimize the setting of cardiac resynchronization therapy? *Europace* 2009; 11: v46-v57

Bland JM, D.G. Altman DG. Statistical methods for assessing agreement between two methods of clinical measurement. *Lancet* 1986; 1: 307-310

Blanco P. Rationale for using the velocity-time integral and minute distance for assessing the stroke volume and cardiac output in point-of-care settings. *Ultrasound J* 2020; 12:21

Bou Chebl R, Dagher GA, Wuhantec J, et al. Mitral valve velocity time integral and passive leg raising as a measure of volume responsiveness. *Crit Ultrasound J* 2018; 10:32

Brabham WW, Gold MR. The role of AV and VV optimization for CRT. *J Arrhythmia* 2013; 29:153-161

Braun MU, Schnabel A, Rauwolf T, et al. Impedance cardiography as a noninvasive technique for atrioventricular interval optimization in cardiac resynchronization therapy. *J Interventional Card Electrophysiol. 2005*; 13:223-229

Chemla D, Demolis P, Thyrault M, et al. Blood flow acceleration in the carotid and brachial arteries of healthy volunteers: respective contributions of cardiac performance and local resistance. *Fundam. Clin. Pharmacol.* 1996; 10:393-399

Chemla D, Levenson, Valensi P, et al. Effect of Beta adrenoceptors and thyroid hormones on velocity and acceleration of peripheral arterial flow in hyperthyroidism. *1990 Am J Cardiol* 1990; 65:494-500, Feb. 1990

Critchley LA, Calcroft RM, Tan PY, et al. The effect of lung injury and excessive lung fluid on impedance cardiac output measurements, in the critically ill. *Intensive Care Med* 2000; 26:679-685

L.A. Critchley LA, Critchley JA. A meta-analysis of studies using bias and precision statistics to compare cardiac output measurement techniques. *J Clin Monit Comput* 1999; 15:85-91

Daubert C, Behar N, Martins RP, et al. Avoiding non-responders to cardiac resynchronization therapy: a practical guide. *Eur Heart J* 2017; 38:1463-1472

Desai AS. Heart failure with preserved ejection fraction. *J Am Coll Cardiol* 2013; 62:272-274

Dillier R, Kobza R, Erne s, et al. Noninvasive detection of left-ventricular systolic dysfunction by acoustic cardiography in atrial fibrillation. *Cardiol Res Pract.* 2011; article ID 173102. 7 pages.

Dupuis JM, Kobeissi A, Vitali L, et al. Programming optimal atrioventricular delay in dual chamber pacing using peak endocardial acceleration: comparison with a standard echocardiographic procedure. *Pacing Clin Electrophysiol* 2003; 26:210-213

Figueroa ML, Peters JI. Congestive heart failure: diagnosis, pathophysiology, therapy, and implications for respiratory care. *Respir Care* 2006; 51:403-412

Gaw RL, B.H. Cornish BH, B.J. Thomas B. The electrical impedance of blood flowing through rigid tubes: a theoretical investigation. *IEEE Trans. Biomed. Eng.* 2008; 55:721-727

Gold MR, Yu Y, Singh JP, et al. Effect of interventricular electrical delay on atrioventricular optimization for cardiac resynchronization therapy. *Circ Arrhythm Electrophysiol* 2018; 11:1-9

Goldhaber JI, Hamilton MA. Role of inotropic agents in the treatment of heart failure. *Circulation* 2010; 121:1655-1660

Hasan A, Abraham WT, Quinn-Tate L, et al. Optimization of cardiac resynchronization devices using acoustic cardiography: a comparison with echocardiography. *CHF* 2006; 12:25-31

Heinroth KM, Elster M, Nuding S, et al. Impedance cardiography: a useful and reliable tool in optimization of cardiac resynchronization devices. *Europace* 2007; 9:744-750

Houthuizen P, Bracke FL. Atrioventricular and interventricular delay optimization in cardiac resynchronization therapy: physiologic principles and overview of available methods. *Heart Fail Rev* 2011; 16:263-276

Inamdar AA, Inamdar AC. Heart failure: diagnosis, management and utilization. *J Clin Med* 2016; 5: 7-28

Khan FZ, Virdee MS, Hutchinson J, et al. Cardiac resynchronization therapy using noninvasive cardiac output measurement. *Pacing Clin Electrophysiol* 2011; 34:1527-1536

Lamberts CR, Nichols WW, Pepine CJ. Indices of ventricular contraction state: comparative sensitivity and specificity. *Am Heart J* 1983; 106:136-144

Lim SH, Lip GY, Sanderson JE. Ventricular optimization of biventricular pacing: a systematic review. *Europace* 2008; 10:901-906

Lee AJ, Cohn JH, Ranasinghe JS, Cardiac output assessed by invasive and minimally invasive techniques. *Anesthesiol Res Pract.* 2011; 2011: 1-15, ID 475151

Lorne E, Mahjoub Y, Diouf M, et al. Accuracy of impedance cardiography for evaluating trends in cardiac output: a comparison with oesophageal Doppler. *Br J Anaesth* 2014; 113:596-602

Melzer C, Borges AC, Knebel F, et al. Echocardiographic AV-interval optimization in patients with reduced left ventricular function. *Cardiovasc Ultrasound* 2004; 2:30

Nazario LR, Silva PM, Pocinho RM, et al. Good agreement between echocardiography and impedance cardiography in the assessment of left ventricular performance in hypertensive patients. *Clin Exp Hypertens* 2018; 40:461-467

Normand C, Linde C, Singh J, et al. Indications for cardiac resynchronization: a comparison of the major international guidelines. *JACC Heart Fail* 2018; 6:308-316

Ovsyshcher I, Zimlichman R, Katz A, et al. Measurements of cardiac output by impedance cardiography in pacemaker patients at rest: effects of various atrioventricular delays. *J Am Coll Cardiol* 1993; 21:761-767

Owen JS, Khatib S, Morin DP. Cardiac resynchronization therapy. *The Ochsner Journal* 2009; 9:248-256

Osypka M. Method and apparatus for automatic determination of hemodynamically optimal cardiac pacing parameter values. US Patent No. US 8,219,195 B2. Date of Patent: Jul 10, 2012

Parmley WW. Pathophysiology of congestive heart failure. *Am J Cardiol* 1985; 56:7A-11

Peyton PJ, Chong SW, Minimally invasive measurement of cardiac output during surgery and critical care: a meta-analysis of accuracy and precision. *Anesthesiology* 2010; 113: 1220-1235

Raaijmakers E, Faes TJ, Kunst PW, et al. The influence of extravascular lung water on cardiac output measurements using thoracic impedance cardiography. *Physiol Meas* 1995;19: 491-499

Rushmer RF. Initial Ventricular Impulse: a potential key to cardiac evaluation. *Circulation* 1964; 29:268-283

Santangeli P, Di Biase L, Pelargonio G, et al. Cardiac resynchronization therapy in patients with mild heart failure: a systematic review and meta-analysis. *J Interv Card Electrophysiol* 2011; 32:125-135

Sawhney NS, Waggoner AD, Garhwal S, et al. Randomized prospective trial of atrioventricular delay programming for cardiac resynchronization therapy. *Heart Rhythm* 2004; 1:562-567

Strickberger SA, Conti J, Daoud EG, et al. Patient Selection for cardiac resynchronization therapy. *Circulation* 2005; 111:2146-2150

Turcott RG, Witteles RM, Wang PJ, et al. Measurement precision in the optimization of cardiac resynchronization therapy. *Circ Heart Fail*. 2010; 3:395-404

Turley AJ, Raja SG, Salhiyyah K, et al. Does cardiac resynchronization therapy improve survival and quality of life in patients with end-stage heart failure? *Interactive CardioVascular and Thoracic Surgery*. 2008; 7:1141-1147

Urbanek B, Chudzik M, Klimczak A, et al. Whether noninvasive optimization of AV and VV delays improves the response to cardiac resynchronization therapy. *Cardiology* J 2013; 4:411-417

Urbanek B Kaczmarek K, Klinczak A, et al. Potential benefit of optimizing atrioventricular and interventricular delays in patients with cardiac resynchronization therapy. *Indian J Med Res* 2017; 146:71-77

Vijayvergiya R, Gupta A. Comparison of echocardiography and device-based algorithm for atrio-ventricular delay optimization in heart block patients. *World J Cardiol* 2015; 26:801-807

Waggoner AD, de las Fuentes L, Davila-Roman VG. Doppler echocardiographic methods for optimization of the atrioventricular delay during cardiac resynchronization therapy. *Echocardiography* 2008; 25:1047-1055

Wang L, Patterson R. Multiple sources of the impedance cardiogram based on 3-D finite difference human thorax models. *IEEE Trans Biomed Eng* 1995; 42:141-148

Wang JJ, Wang PW, Liu CP, et al. Evaluation of changes in cardiac output from the electrical impedance waveform in the forearm. *Physiol Meas* 2007; 28:989-999

Wang JJ, Hu WC, Kao J, et al. Development of forearm plethysmography for minimally invasive monitoring of cardiac pumping function. J Biomedical Science and engineering 2011; 4:122-129

Wang L. Cardiac resynchronization therapy in congestive heart failure: The state of the art and future perspectives. *Exp Clin Cardiol* 2003; 7:212-215

Whinnett ZI, Davies JE, Wilson K, et al. Determination of optimal atrioventricular delay for cardiac resynchronization using acute non-invasive blood pressure. *Europace* 2006; 8:358-366

Yu CM, Chau E, Sanderson JI. Tissue Doppler echocardiographic evidence of reverse modeling and improved synchronicity by simultaneously delaying regional contraction after biventricular pacing therapy in heart failure. *Circulation* 2002; 105:438-445